Research Article | Vol. 24, No. 24 | 28 Nov 2016 | OPTICS EXPRESS 27812

Optics EXPRESS

Single longitudinal mode diamond Raman laser in the eye-safe spectral region for water vapor detection

OLIVER LUX,[1,2,*] SOUMYA SARANG,[1] ROBERT J. WILLIAMS,[1] AARON MCKAY,[1] AND RICHARD P. MILDREN[1]

[1]*MQ Photonics Research Centre, Faculty of Science and Engineering, Macquarie University, New South Wales 2109, Australia*
[2]*Deutsches Zentrum für Luft- und Raumfahrt (DLR), Institut für Physik der Atmosphäre, Oberpfaffenhofen 82234, Germany*
**oliver.lux@dlr.de*

Abstract: We report a narrowband and tunable diamond Raman laser generating eye-safe radiation suitable for water vapor detection. Frequency conversion of a tunable pump laser operating from 1063 to 1066 nm to the second order Stokes component in an external standing-wave cavity yielded 7 W of multimode output power in the wavelength range from 1483 to 1488 nm at a conversion efficiency of 21%. Stable single longitudinal mode operation was achieved over the whole tuning range at low power (0.1 W), whereas incorporation of a volume Bragg grating as an output coupler enabled much higher stable power to be attained (0.5 W). A frequency stability of 40 MHz was obtained over a minute without active cavity stabilization. It was found that mode stability is aided via seeding of the second Stokes by four-wave mixing, which leads to a doubling of the mode-hopping interval. The laser was employed for the detection of water vapor in ambient air, demonstrating its potential for remote sensing applications.

OCIS codes: (140.3550) Lasers, Raman; (140.3570) Lasers, single-mode; (140.3600) Lasers, tunable; (050.7330) Volume gratings; (010.3640) Lidar.

References and links

1. A. Fix, C. Büdenbender, M. Wirth, M. Quatrevalet, A. Amediek, C. Kiemle, and G. Ehret, "Optical parametric oscillators and amplifiers for airborne and spaceborne active remote sensing of CO_2 and CH_4," Proc. SPIE **8182**, 818206 (2011).
2. M. Wirth, A. Fix, P. Mahnke, H. Schwarzer, F. Schrandt, and G. Ehret, "The airborne multi-wavelength water vapor differential absorption lidar WALES: system design and performance," Appl. Phys. B **96**(1), 201–213 (2009).
3. A. Fix, M. Quatrevalet, B. Witschas, M. Wirth, C. Büdenbender, A. Amediek, and G. Ehret, "Challenges and solutions for frequency and energy references for spaceborne and airborne integrated path differential absorption lidars," *Proceedings of the 27th International Laser Radar Conference*, (New York, 2015)
4. M. J. Livrozet, F. Elsen, J. Wüppen, J. Löhring, C. Büdenbender, A. Fix, B. Jungbluth, and D. Hoffmann, "Feasibility and performance study for a space-borne 1645 nm OPO for French-German satellite mission MERLIN," Proc. SPIE **8959**, 89590G (2014).
5. M. Němec, J. Šulc, L. Indra, M. Fibrich, and H. Jelínková, "Tunable eye-safe Er:YAG laser," Laser Phys. **25**(1), 15803 (2015).
6. B. Q. Yao, T. Y. D. Deng, X. M., Duan, Y. L. Ju, and Y. Z. Wang, "Tunable single-longitudinal-mode Er:YAG laser using a twisted-mode technique at 1.6 μm," Laser Phys. Lett. **12**(2), 25004 (2015).
7. P. Tang, J. Liu, B. Huang, C. Xu, C. Zhao, and S. Wen, "Stable and wavelength-locked Q-switched narrow-linewidth Er:YAG laser at 1645 nm," Opt. Express **23**(9), 11037–11042 (2015).
8. H. Fritsche, O. Lux, X. Wang, Z. G. Zhao, and H. J. Eichler, "Resonantly diode pumped Er:YAG laser systems emitting at 1645 nm for methane detection," Laser Phys. Lett. **10**(10), 105805 (2013).
9. O. Lux, H. Rhee, H. Fritsche, and H. J. Eichler, "Barium nitrate Raman laser at 1.599 μm for CO_2 detection," Proc. SPIE **8677**, 86771B (2013).
10. J. T. Murray, W. L. Austin, and R. C. Powell, "Intracavity Raman conversion and Raman beam cleanup," Opt. Mater. **11**(4), 353–371 (1999).
11. O. Lux, S. Sarang, O. Kitzler, D. J. Spence, and R. P. Mildren, "Intrinsically stable high-power single longitudinal mode laser using spatial hole burning free gain," Optica **3**(8), 876–881 (2016).

#275656 http://dx.doi.org/10.1364/OE.24.027812
Journal © 2016 Received 29 Sep 2016; revised 10 Nov 2016; accepted 10 Nov 2016; published 21 Nov 2016

Optics EXPRESS

12. R. J. Williams, J. Nold, M. Strecker, O. Kitzler, A. McKay, T. Schreiber, and R. P. Mildren, "Efficient Raman frequency conversion of high-power fiber lasers in diamond," Laser Photonics Rev. **9**(4), 405–411 (2015).
13. A. McKay, O. Kitzler, and R. P. Mildren, "Simultaneous brightness enhancement and wavelength conversion to the eye-safe region in a high-power diamond Raman laser," Laser Photonics Rev. **8**(3), L37–L41 (2014).
14. A. McKay, H. Liu, O. Kitzler, and R. P. Mildren, "An efficient 14.5 W diamond Raman laser at high pulse repetition rate with first (1240 nm) and second (1485 nm) Stokes output," Laser Phys. Lett. **10**(10), 105801 (2013).
15. W. Lubeigt, V. G. Savitski, G. M. Bonner, S. L. Geoghegan, I. Friel, J. E. Hastie, M. D. Dawson, D. Burns, and A. J. Kemp, "1.6 W continuous-wave Raman laser using low-loss synthetic diamond," Opt. Express **19**(7), 6938–6944 (2011).
16. J.-P. M. Feve, K. E. Shortoff, M. J. Bohn, and J. K. Brasseur, "High average power diamond Raman laser," Opt. Express **19**(2), 913–922 (2011).
17. D. C. Parrotta, A. J. Kemp, M. D. Dawson, and J. E. Hastie, "Multiwatt, continuous-wave, tunable diamond Raman laser with intracavity frequency-doubling to the visible region," IEEE J. Sel. Top. Quantum Electron. **19**(4), 1400108 (2013).
18. E. S. Chung, B. Soden, B. J. Sohn, and L. Shi, "Upper-tropospheric moistening in response to anthropogenic warming," Proc. Natl. Acad. Sci. U.S.A. **111**(32), 11636–11641 (2014).
19. L. B. Glebov, "High-performance solid-state and fiber lasers controlled by volume Bragg gratings," Rev. Laser Eng. **41**(9), 684–690 (2013).
20. H. Jasbeer, R. J. Williams, O. Kitzler, A. McKay, S. Sarang, J. Lin, and R. P. Mildren, "Birefringence and piezo-Raman analysis of single crystal CVD diamond and effects on Raman laser performance," J. Opt. Soc. Am. B **33**(3), B56–B64 (2016).
21. R. J. Williams, D. J. Spence, O. Lux, and R. P. Mildren, "High-power continuous-wave Raman frequency conversion from 1.06 μm to 1.49 μm in diamond," Opt. Express ID 280855 (posted 14 November 2016, under review).
22. L. S. Rothman, I. E. Gordon, Y. Babikov, A. Barbe, D. Chris Benner, P. F. Bernath, M. Birk, L. Bizzocchi, V. Boudon, L. R. Brown, A. Campargue, K. Chance, E. A. Cohen, L. H. Coudert, V. M. Devi, B. J. Drouin, A. Fayt, J.-M. Flaud, R. R. Gamache, J. J. Harrison, J.-M. Hartmann, C. Hill, J. T. Hodges, D. Jacquemart, A. Jolly, J. Lamouroux, R. J. Le Roy, G. Li, D. A. Long, O. M. Lyulin, C. J. Mackie, S. T. Massie, S. Mikhailenko, H. S. P. Müller, O. V. Naumenko, A. V. Nikitin, J. Orphal, V. Perevalov, A. Perrin, E. R. Polovtseva, C. Richard, M. A. H. Smith, E. Starikova, K. Sung, S. Tashkun, J. Tennyson, G. C. Toon, V. G. Tyuterev, and G. Wagner, "The HITRAN 2012 molecular spectroscopic database," J. Quant. Spectrosc. Radiat. Transf. **130**, 4–50 (2013).
23. T. L. Nicholson, S. L. Campbell, R. B. Hutson, G. E. Marti, B. J. Bloom, R. L. McNally, W. Zhang, M. D. Barrett, M. S. Safronova, G. F. Strouse, W. L. Tew, and J. Ye, "Systematic evaluation of an atomic clock at 2 × 10(-18) total uncertainty," Nat. Commun. **6**, 6896 (2015).

1. Introduction

Powerful eye-safe lasers with high spectral purity are required for active remote sensing of atmospheric trace gases. In particular, air- and space-borne light detection and ranging (lidar) systems aiming at accurate concentration measurements of the most important greenhouse gases (GHGs) carbon dioxide, methane and water vapor rely on high-power, frequency-stable laser sources emitting at specific absorption lines of the measured gas species. In order to meet the stringent demands in terms of power performance as well as of the spectral and spatial laser properties, injection-seeded optical parametric oscillators (OPOs) and amplifiers (OPAs) are currently employed as laser transmitters [1,2]. For instance, OPO/OPA systems operating at 1571 nm and 1645 nm have been developed for the air-borne lidar system CHARM-F which allows for simultaneous measurement of carbon dioxide and methane column concentrations [3]. A similar laser transmitter will be realized for the upcoming German-French satellite mission MERLIN (Methane Remote Sensing Lidar Mission) which strives for precise quantification of spatial and temporal gradients of atmospheric methane columns with low bias [4]. In recent years, resonantly pumped Er:YAG lasers have been investigated as an alternative for carbon dioxide and methane detection. Here, the laser directly operates at 1617 nm or 1645 nm which enables higher efficiency and smaller footprint of the overall system [5–8]. However, both concepts based on OPOs and Er:YAG lasers exhibit deficiencies regarding the beam quality, especially at high power levels due to thermally-induced beam distortions.

Another promising approach for realizing lidar transmitters is provided by Raman lasers which allow for efficient frequency conversion of mature laser systems to selected emission wavelengths suitable for trace gas detection [9]. Apart from their compactness, major

Optics EXPRESS

advantages of Raman lasers are derived from the automatic phase matched nature of stimulated Raman scattering, which diminishes thermal dephasing and enables Raman beam-cleanup [10]. The latter describes the fact that the spatial gain profile experienced by the generated Stokes beam is a convolution of the pump and Stokes fields which converges to a Gaussian distribution, thus providing fundamental transverse mode (TEM_{00}) output and diffraction limited beam quality.

Furthermore, recent studies have shown that single longitudinal mode (SLM) operation, which is a prerequisite for narrowband laser emission, can be readily obtained in standing-wave Raman lasers without the use of line selective elements due to the lack of spatial hole burning [11]. From the multitude of Raman crystals, CVD diamond has been demonstrated to be an excellent material for high-power frequency conversion due to its high Raman gain coefficient and its beneficial thermo-mechanical properties, which in combination with the Raman beam cleanup effect, avoids detrimental thermal lensing and offers high-brightness output [12–16]. Following this approach, efficient eye-safe laser generation was obtained in a diamond Raman laser, providing 16 W power at 1485 nm with near-diffraction-limited beam quality [13]. Furthermore, intracavity frequency-doubling of a cw diamond Raman laser has been accomplished, yielding watt-level, tunable output with excellent beam quality in the visible spectral region [17].

In this study, we show that, aside from their excellent power and beam quality performance, diamond Raman lasers additionally allow for the generation of frequency-stable and narrowband output at selected GHG absorption lines in the near-infrared spectral region. For this purpose, an external cavity diamond Raman laser operating in SLM was developed which was tunable from 1483 to 1488 nm, while water vapor in the ambient air was chosen as absorbing gas species to demonstrate the laser's potential for trace gas detection. Water vapor is the principal GHG due to its large atmospheric abundance and its role as a key amplifier of global warming [18]. Precise measurement of the atmospheric water vapor concentration is therefore essential to check and improve climate models and to provide more accurate climate change and weather predictions.

In the course of our investigations, we studied the influence of a volume Bragg grating (VBG) on the spectral properties of the Raman laser. VBGs are rapidly emerging as compact and robust optical elements for spectral narrowing and mode-selection in all types of lasers [19]; however, until now their applicability in crystalline Raman lasers has not been demonstrated. Finally, we show that the effective mode spacing of a SLM Raman laser scales with the Stokes order, thus benefiting the stability of single-mode operation in higher-order Stokes Raman lasers.

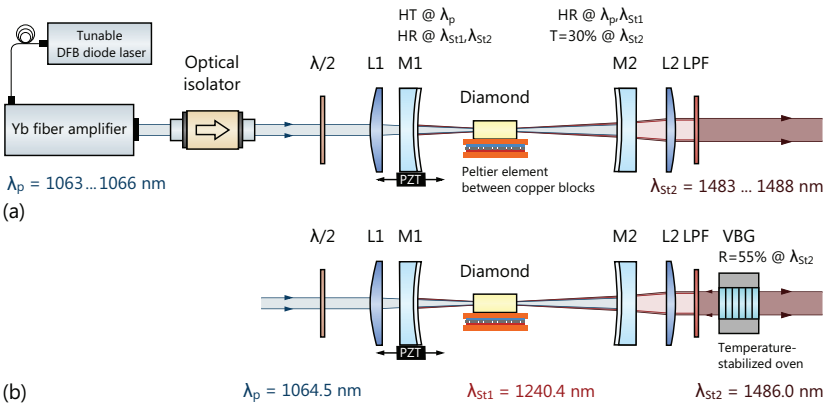

Fig. 1. Experimental setup of the second Stokes Raman lasers: (a) single-cavity configuration for tunable output from 1483 to 1488 nm, (b) coupled-cavity configuration employing a volume Bragg grating (VBG).

Optics EXPRESS

2. Experimental setup and Raman laser performance

The experimental setup of the tunable external cavity second Stokes Raman laser is depicted in Fig. 1(a). A single-frequency distributed feedback (DFB) laser (TOPTICA Photonics, model DL DFB BFY), amplified by an Yb fiber amplifier (IPG Photonics, model YAR-LP-SF), was employed as a pump source, delivering up to 40 W cw output power at diffraction-limited beam quality (M^2 = 1.05) and high frequency stability (40 MHz over one hour). The pump wavelength was tunable in the range from 1062.8 to 1065.6 nm by varying the operating temperature of the DFB laser with a thermal tuning rate of 80 pm/K. Optical feedback between the pump and the Raman laser was prevented by using an optical isolator, while a half-wave plate was utilized to ensure polarization of the pump radiation along the [111] axis of the diamond, thus providing highest Raman gain [20].

A plano-convex lens with f_{L1} = 50 mm focal length was used to focus the pump beam into the low-nitrogen, low-birefringence, CVD-grown single-crystal diamond (ElementSix, Ltd.) which was placed on a copper block in the center of a near-concentric optical cavity, resulting in a pump spot diameter in the diamond of about 66 µm. The rectangular crystal with dimensions of 8 mm × 4 mm × 1.2 mm was anti-reflection-coated at the first and second Stokes wavelength showing transmission of 99.5% at 1.24 µm and 98.9% at 1.48 µm, respectively.

The Raman oscillator was formed by two concave mirrors with radii of curvature of 50 mm and 75 mm, respectively. The mirrors were spaced by 125 mm, leading to an optical cavity length of 136 mm considering the refractive index of the diamond. Both mirrors were highly reflective at the first Stokes wavelength ($R_{M1}(\lambda_{St1})\approx 99.95\%$, $R_{M2}(\lambda_{St1})\approx 99.99\%$), generating intracavity first Stokes field powers in the kW range. The input coupler (M1) also highly reflected the second-order Stokes radiation ($R_{M1}(\lambda_{St2})\approx 99.0\%$), while the output coupler (M2) partially transmitted this component ($T\approx 30\%$). The choice of mirror specifications, especially high output coupling at the second Stokes wavelength, were based on insights recently gained from analytical modeling of cw external-cavity Raman lasers [21].

Measurement of the laser performance showed low threshold (6 W) for both first and second Stokes generation, while the first Stokes power remained nearly constant once the second Stokes field arose, as displayed in Fig. 2(a). Above the second Stokes threshold, the first Stokes field merely acts as a mediator between the pump and the second Stokes fields, so that efficient conversion to the latter is achieved [21]. The maximum second Stokes power was measured to be 7 W at 34 W pump power, corresponding to a conversion efficiency of 21%.

The output wavelength was continuously tunable by varying the temperature of the DFB pump laser diode, realizing a tuning range from 1483 to 1488 nm. The spectral characteristics of the Raman laser emission were studied using a laser spectrum analyzer (Bristol Instruments, model 771) with a wavelength accuracy of 30 MHz at 1.48 µm. Here, the transition from multimode to single-mode operation was readily observed by the appearance of a smooth Lorentzian line shape as well as a significant reduction of the frequency fluctuations from several GHz to a few tens of MHz, as shown in Fig. 2(b). SLM operation of the Raman laser was obtained for output powers up to approximately 0.1 W. However, multimode operation was observed at higher powers. Thermally induced changes in Raman shift and optical path length are considered to be the major reason for limiting the SLM power [11]. Thermal loading of the diamond is aggravated compared to the first Stokes Raman laser due to the strong intracavity first Stokes field (hence larger impurity absorption) and the additional heat load due to the cascaded Stokes process. This stronger coupling between Stokes power and optical cavity length results in a reduced maximum SLM output power compared to that observed for a first Stokes laser (up to 4 W [11]).

Optics EXPRESS

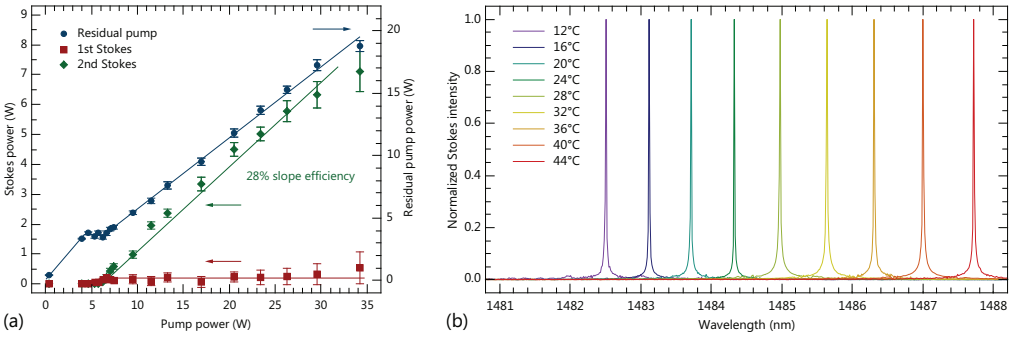

Fig. 2. Performance of the second Stokes diamond Raman laser: (a) Output power of the first and second Stokes radiation as well as residual pump power versus pump power, (b) Raman laser spectrum depending on the temperature of the DFB pump laser diode.

3. Wavelength stabilization using a volume Bragg grating

To increase the SLM power and to improve the frequency stability on longer time scales, a volume Bragg grating (VBG) (OptiGrate Corp) was incorporated into the system, according to the scheme in Fig. 1(b), by placing it 100 mm behind mirror M2. The VBG was designed to have a peak diffraction efficiency (reflectivity) of 55% at 1486.0 nm wavelength at normal incidence with a reflection bandwidth of about 100 pm (FWHM). In this way, it acted as the second Stokes output coupler and formed a coupled cavity of about 250 mm optical length with the inner cavity formed by M1 and M2. A plano-convex lens (f_{L2} = 75 mm, AR-coated at λ_{St2}), which was placed at a distance of 25 mm from M2, collimated the beam onto the VBG to facilitate a stable resonator mode, while a long-pass filter (LPF), which was highly transmitting at the second Stokes wavelength ($T \approx 84\%$), was utilized to suppress the pump and first Stokes radiation leaking through the inner cavity. Wavelength tuning of the VBG-stabilized Raman laser was accomplished by scanning the pump laser wavelength in combination with heating the grating in a temperature-controlled oven. The latter allowed shifting the VBG peak wavelength from 1486.0 to 1486.6 nm with an accuracy of about 1 pm (135 MHz).

The influence of the VBG on the spectral purity of the Raman laser was investigated by recording its spectrum for the second Stokes tuned on- and off-resonance with the grating peak. Figure 3(a) shows both cases, measured at 0.5 W output power. Multimode operation was evident when the Raman laser was tuned off-resonance so that the VBG was transparent for the second Stokes radiation, leading to side-bands in the Raman laser output spectrum and frequency fluctuations of about 4 GHz. In contrast, oscillation of a single longitudinal mode was observed when the pump laser wavelength was set such that the second Stokes wavelength matched the room temperature VBG peak wavelength at 1486.00 nm and optical feedback was provided. As depicted in Fig. 3(b), the stability of the center wavelength was about 40 MHz over periods of one to two minutes, which is in the order of the pump frequency fluctuations. Hence, the utilization of the VBG facilitates SLM operation as it improves the mode discrimination despite its broad bandwidth of about 100 pm.

Optics EXPRESS

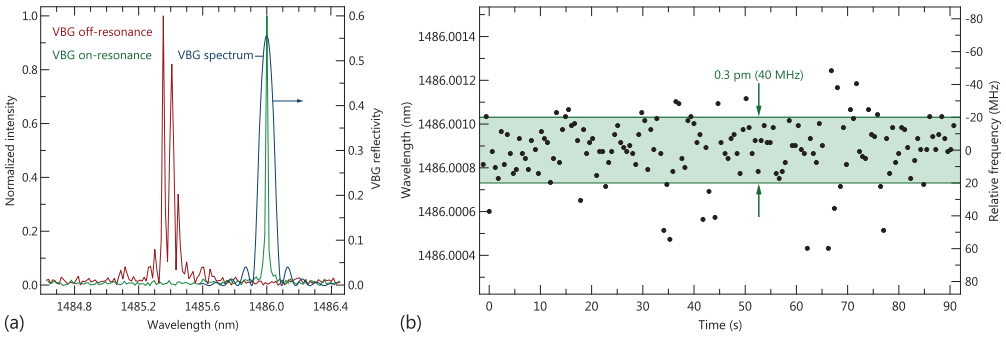

Fig. 3. Spectral properties of the second Stokes diamond Raman laser: (a) Stokes output spectra with and without optical feedback from the volume Bragg grating (VBG). (b) Temporal fluctuations of the center wavelength measured at 0.5 W Stokes power.

As shown in Fig. 4, measurement of the temporal variation of the center wavelength over several minutes revealed the occurrence of mode-hops which is attributed to heating of the diamond and its mount. Owing to the aforementioned impurity absorption and Stokes generation, the diamond and mount increases in temperature by tens of Kelvin within a few minutes, which leads to an increase of the optical path length and alters the Raman shift frequency [11]. In principle, this problem can be readily overcome by active cooling of the diamond mount. The mode-hops were measured to be (1.8 ± 0.2) GHz which corresponds to twice the mode spacing of the inner first Stokes cavity. The reason for this is explained as follows.

In the case of the first Stokes mode, the frequency is an integer multiple of the inner cavity mode spacing Δv and lies close to the peak of the Raman gain near 1240 nm. The second Stokes mode will experience gain due to the first Stokes field as its pump, and be seeded by spontaneous Raman scattering and the result of non-phase-matched four-wave mixing (FWM) of the fundamental frequency v_0 with the first Stokes frequency $v_{St1} = v_0 - n \cdot \Delta v$, where n is a positive integer. While the former process potentially seeds all cavity modes, the latter only provides a seed at $2v_{St1} - v_0 = v_0 - 2n \cdot \Delta v$ due to energy conservation. Hence, we deduce from the observed mode-hop interval of $2\Delta v$ that four-wave mixing is the dominant seeding mechanism. It should be noted that the above explanation presumes that the optical lengths of the coupled cavities formed by M1 and M2, and M1 and the VBG are chosen such that the cavities are in resonance. However, due to the low finesse of the latter which is further diminished by intracavity losses introduced by lens L2 and the long-pass filter, the exact cavity lengths are not critical for stable SLM operation.

The concept of increased mode spacing may be transferrable to higher Stokes orders. As the frequency of the mth Stokes order is seeded by FWM, spaced from the fundamental by $m \cdot n \cdot \Delta v$, the number of available longitudinal modes within the Raman gain bandwidth is reduced by factor m. This may be a useful feature, as it enables secondary modes to be more easily discriminated, e.g. by the gain profile or inserted frequency selective cavity elements, and thus assists in SLM stability.

Optics EXPRESS

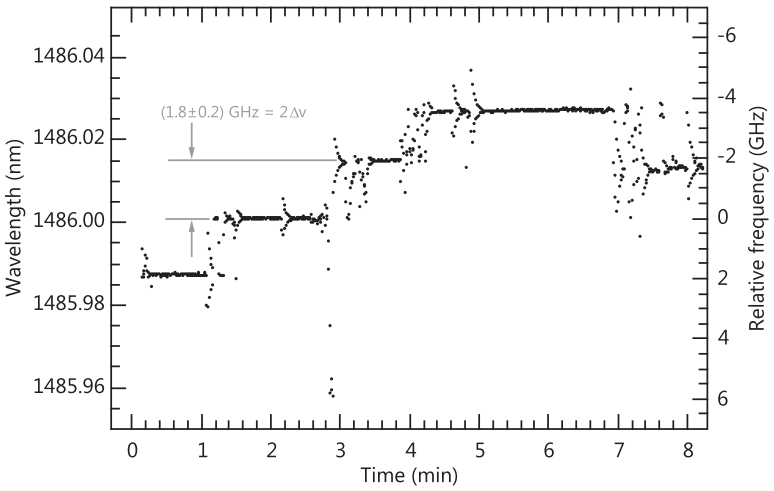

Fig. 4. Mode-hopping of the second Stokes diamond Raman laser.

4. Water vapor absorption measurements

The suitability of the second Stokes SLM diamond Raman laser for LIDAR applications was verified by performing absorption measurements of water in air. For this purpose, the output beam of the Raman laser was first separated into two portions, as depicted in Fig. 5. While a weak part was guided to a laser spectrum analyzer which monitored the temporal variation of the radiation wavelength, the major part passed through a mechanical chopper and propagated through the lab over a path length of a few meters before being incident on an InGaAs photodiode. The chopper-modulated output signal was fed into a lock-in amplifier together with the chopper frequency to increase the signal-to-noise ratio of the transmitted signal. A second photodiode, placed close to the coupling lens of the spectrum analyzer, provided a reference signal. The path length difference between the "reference beam" and the "transmitted beam" was 3.8 m. The temporal evolution of the ratio between the transmitted and reference signal was measured simultaneously with the wavelength variations to determine the correlation between laser wavelength and water vapor absorption.

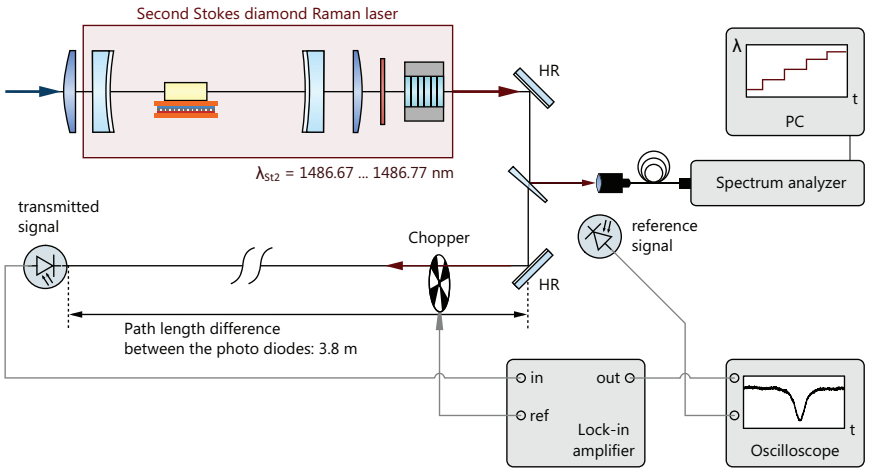

Fig. 5. Experimental setup for measuring water absorption in the spectral region around 1486.7 nm using the tunable SLM second Stokes diamond Raman laser.

Optics EXPRESS

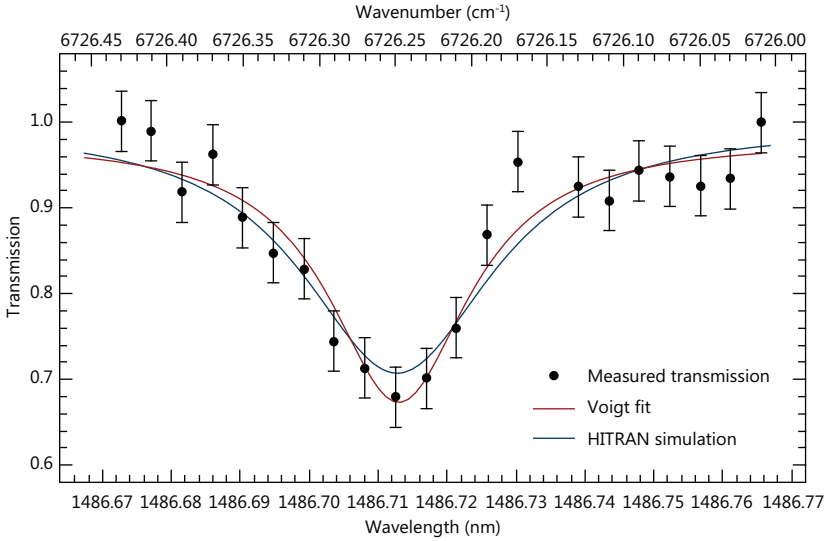

Fig. 6. Measured transmission of the Raman laser through air together with a Voigt profile fit and calculated transmission based on spectroscopic data from the HITRAN database [22].

The laser was tuned to a H_2O absorption line at 1486.713 nm (6726.2488 cm^{-1}), which was the strongest line in the tuning range of the Raman laser. However, it was located outside of the VBG tuning range, making it difficult to sustain stable mode-hop free operation on longer time scales. The temperature and relative humidity in the laboratory were measured to be $T = 20.0$°C and $r \approx 60\%$, corresponding to a water vapor partial pressure of about 14 mbar. The simulated transmission spectrum for the given experimental parameters and using spectroscopic data from the HITRAN database [22] is plotted in Fig. 6. Due to self- and air-broadening of the absorption line, the FWHM of the profile accounts for about 0.15 cm^{-1} (4.5 GHz), while the minimum transmission is in the range of 75%. These values were within the error margins of the experimental data which was obtained by averaging the measured relative transmission in wavenumber bins of width 0.02 cm^{-1}. Thus, the developed Raman laser was demonstrated to be feasible for water vapor detection.

5. Conclusion

We have demonstrated SLM operation of a diamond Raman laser emitting in the eye-safe spectral region. Efficient frequency conversion of a tunable pump laser to the second order Stokes component produces 7 W multimode output power in the range from 1483 to 1488 nm. Implementation of a volume Bragg grating increased the single-mode output power from 0.1 W to 0.5 W, while improving the frequency stability over time scales of several minutes. Analysis of the long-term frequency stability revealed that the effective mode spacing of the Raman laser is twice the cavity mode spacing which can be explained by seeding of the second Stokes by four-wave mixing and represents a beneficial inherent property of higher-order Raman lasers when aiming at SLM operation. Finally, the Raman laser was successfully employed for water vapor detection. Here, significant reduction of the measurement error is expected by improving the laser frequency stability, e.g. by using a VBG whose room temperature peak wavelength matches the center wavelength of the selected absorption line.

Detection of other gas species can be accomplished by adapting the current system to use a greater fraction of the Yb fiber amplifier gain spectrum (e.g. from 1010 to 1120 nm), thus enabling access to major portions of the near-infrared via first (1165 – 1320 nm) and second Stokes (1380 – 1600 nm) generation. Therefore, it is expected that SLM Raman lasers based on the developed concept represent a promising alternative to existing OPO/OPA and erbium-based laser sources applied for remote sensing of atmospheric gases.

Optics EXPRESS

With a view to their applicability in lidar systems, Raman lasers offer higher spectral brightness than erbium lasers of comparable complexity which show either lower SLM output powers ranging from tens to a few hundred mW [5,6] or lower spectral purity [8]. Compared to the currently employed OPO/OPA systems, Raman lasers are superior in terms of compactness and beam quality. The latter is diminished in OPOs and OPAs especially at elevated power levels, owing to thermally induced aberrations in the nonlinear crystal which lead to M^2 values in the order of 2 [1]. In contrast, the Raman beam-cleanup effect enables diffraction-limited output in the eye-safe spectral region even at high output powers beyond 100 W [21].

In general, the potential for power scaling, especially of diamond Raman lasers, opens new opportunities for developing high-power SLM lasers which are of great interest not only for remote sensing applications, but also for other research areas such as gravitational wave detection and laser cooling. Furthermore, extension of the available emission wavelengths to the visible spectral range can be achieved by subsequent second harmonic generation, reaching, for instance, 698 nm which represents the wavelength of the $^1S_0 \rightarrow {}^3P_0$ clock transition in Sr atomic clocks [23].

Future investigations will primarily aim to implement active cavity length control to enhance stabilization, e.g. by applying the Hänsch-Couillaud method. In particular, the further development of the proposed concept strongly depends on the need to compensate for thermally-induced changes in optical length of the Raman crystal so that stable SLM operation is achieved on longer time scales.

Funding

German Research Foundation (DFG) (LU 2018/1-1); US Air Force Research Laboratory (FA2386-15-1-4075).

Acknowledgments

This work was performed in the laboratories of MQ Photonics Research Centre. The authors would like to thank H. M. Pask, A. J. Lee, and Y. Zheng as well as P. Ha, B. Orr, and Y. He for the loan of spectral characterization equipment and their help with the absorption measurements. R. Williams acknowledges the support of a Macquarie University Research Fellowship.